Scientia Iranica B (2011) 18 (4), 913–922

Sharif University of Technology

Scientia Iranica

Transactions B: Mechanical Engineering

www.sciencedirect.com

Laminar premixed V-shaped flame response to velocity and equivalence ratio perturbations: Investigation on kinematic response of flame

R. Riazi, M. Farshchi *

Department of Aerospace Engineering, Sharif University of Technology, Tehran, P.O. Box 11155-8639, Iran

Received 25 September 2010; revised 26 March 2011; accepted 6 June 2011

KEYWORDS

V-flame;
Equivalence ratio perturbation;
Velocity perturbation;
Flame speed;
Heat of reaction;
Strouhal number.

Abstract The response of a rod-stabilized, V-shaped, premixed flame to upstream velocity and equivalence ratio perturbations was characterized as a function of excitation frequency. The response of the flame to equivalence ratio perturbations was calculated, assuming that the heat release response is controlled by contributions from three disturbances. These disturbances include flame speed, heat of reaction and flame area. Using an analytical model, based on linearization of the front tracking equation for inclined flames, the kinematics of a V-flame anchored on a central obstacle was investigated and its response was compared with that of a conical flame. The results suggest that the phase response of the V-flame increases quasi-linearly with excitation frequency, indicating that the fluctuations require a certain time to reach the flame surface. Longer V-flames exhibit more sensitivity to the convected flow disturbances. The stronger contribution of the flame-area perturbations in the case of a V-flame, which is due to the intensified effect of displacement at the tip of the flame, leads to higher values of the overall response of the flame, compared with that of the conical flame. The flame response to equivalence ratio perturbations indicates that V-flames behave as an amplifier at a certain range of frequencies, and they are more susceptible to flow oscillations than conical flames.

1. Introduction

To meet the stringent regulations regarding permissible emission levels, reduction of NOx emission should be considered a major factor in the design process of gas turbine combustors. Lean premixed combustion decreases the adiabatic flame temperature and consequently reduces the production rate of NOx emission, which is highly temperature dependent [1]. However, in this operating range, the appearance of thermo-acoustic oscillations becomes a major concern. These oscillations have adverse effects on performance [2–5] and can substantially reduce hot section part life [6].

In order to analyze these combustion oscillations, a relevant description of the flame response to flow perturbations should be provided. This can be obtained by determining the transfer function, which describes the amplitude and phase response characteristics of a flame to equivalence ratio and velocity perturbations [3,5] at the linear limit. Candel [3] and Lieuwen [7] have extensively reviewed studies on premixed flame-flow interactions. Some major mechanisms that have been reported to have a significant impact on combustion oscillations are flame area fluctuations driven by acoustic velocity perturbations [8,9] and equivalence ratio oscillations [10]. To gain a better understanding of flame dynamics, various analytical [8,9,11], computational [12,13] and experimental [9] investigations have been done on premixed flame-flow interactions in simple flame geometries.

In experiments, the flame heat release response to the imposed oscillations is usually determined by flame CH* chemiluminescence. Chaparro et al. [14] measured the global spontaneous emission of CH* radicals of flame to calculate the heat release response of premixed *V*-flames to periodic upstream velocity oscillations. They reported [14] that the

* Corresponding author.
E-mail address: farshchi@sharif.edu (M. Farshchi).

1026-3098 © 2011 Sharif University of Technology. Production and hosting by Elsevier B.V. Open access under CC BY-NC-ND license.
Peer review under responsibility of Sharif University of Technology.

doi:10.1016/j.scient.2011.07.002

Production and hosting by Elsevier

flame heat release amplitude response is confined to the low-frequency range of excitation. Schuller et al. [15] studied the response of laminar V-flames and conical flames anchored on an experimental annular burner. In their study [15], the conical flame, which features relatively weaker and slower variations of its surface, was reported to be less likely to excite the acoustical mode of the burner. Durox et al. [16] characterized the nonlinear features of the flame response to velocity perturbations by measuring the flame transfer function in four different geometries: conical flame, V-flame, M-flame and a Collection of Small Conical Flames (CSCF) stabilized on a perforated plate. This study [16] showed that the response notably depends on the steady-state configuration of the flame.

In theoretical studies, flame displacement is modeled by propagation of an infinitely thin interface (flame surface), which separates the unburned gas mixture from products. The total heat release rate is assumed to be controlled by variations in the area of this flame surface that can be determined by the so-called G-equation, which is a front tracking equation for the flame position. Using this approach, Fleifil et al. [8] examined the response of a conical laminar flame stabilized by a ring in a cylindrical duct, with a uniform distribution of acoustic velocity along the flame axis. They showed [8] that the flame behaves like a high-pass filter, in the sense that high-frequency oscillations pass through the flame without significantly affecting the heat-release rate. Low-frequency oscillations, on the other hand, exert a strong influence on the heat-release fluctuation, as shown in their study [8].

Schuller et al. [12] studied the response of two different configurations of laminar flame to the incident velocity perturbations; conical or Bunsen flames anchored by the rim of a circular duct and a V-flame anchored by a central rod in a duct. They showed [12] that flame dynamics are governed by two parameters: a reduced frequency or equivalently the flame Strouhal number and the flame angle with respect to the flow direction. Based on some related experimental studies [17,18], Schuller et al. [12] suggested that the velocity perturbation is nonuniform along the flame front. This was proposed due to the significant difference between theoretical and experimental results, regarding calculation of the flame transfer function at higher ranges of Strouhal number [9,19]. By considering a model with a uniform distribution of velocity perturbation and an axial convective wave along the flame, they showed [12] that the kinematic approach might be extendable to higher frequencies.

Several investigations [20–22] have been done to model the premixed flame response to equivalence ratio perturbations. Cho and Lieuwen [20] studied the dependence of the equivalence ratio-heat release transfer function upon the Strouhal number and flame characteristics, for the case of a conical flame. They suggested that the heat release response is controlled by the contribution of three disturbances:

1. Fluctuations in the heat of reaction of the incoming mixture.
2. Fluctuations in burning velocity affecting the local heat release per unit flame area.
3. Perturbations of the flame surface area induced by fluctuations in the burning velocity.

In the same way, You et al. [23] investigated the combustion response of turbulent premixed flames to flow disturbances. They examined two different configurations; a simple flame and an enveloped flame that are mostly observed in swirl-stabilized combustors [24]. They studied the direct effects of flame speed and heat of reaction oscillations on the unsteady heat release

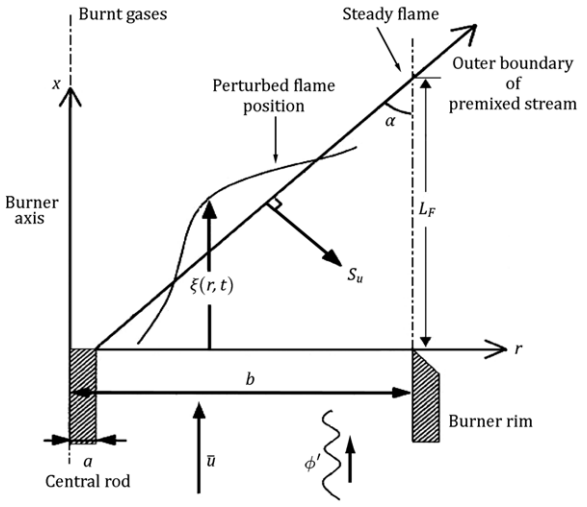

Figure 1: Schematic of V-flame geometry used for determination of the flame transfer function. a: Radius of central rod; b: burner radius, α: flame angle with respect to the mean flow direction.

fluctuation due to the equivalence ratio disturbances. However, they did not consider the indirect effects of flame speed perturbations on heat release fluctuations, which are accomplished through the generation of fluctuations in the flame surface area.

Motivated by these, and considering the fact that the response of the V-flame to equivalence ratio perturbations has not yet been studied analytically, the objective of the present study was to determine the response of a V-flame to upstream velocity and equivalence ratio oscillations, in terms of flame transfer function dependence upon Strouhal number and the flame angle. Direct effects of flame speed and the heat of reaction perturbations on the flame's heat release, together with the indirect effect of flame speed, were considered in this study to compare the flame response characteristics of a V-flame with that of a conical flame.

2. Analysis

To model the flame's response, an analysis similar to that of Fleifil et al. [8] and Cho and Lieuwen [20] was used in this study. The V-flame geometry is illustrated in Figure 1. The principle assumptions of the analysis are [20]:

1. The flame is a thin sheet separating the cold reactants and hot products.
2. The flame is axisymmetric.
3. The flame base remains anchored at its attachment point (i.e., its position does not fluctuate).
4. Flame displacement is described as a single valued function, with respect to radial coordinate.
5. The Mach number of the mean flow is very small ($M \ll 1$).

Considering the assumptions 1, 2, and 4, the kinematic relation describing the flame position as a function of the flow velocity and flame speed is described by the following front tracking equation [12,20]:

$$\frac{\partial \xi}{\partial t} = u - v\frac{\partial \xi}{\partial r} - S_u\sqrt{\left(\frac{\partial \xi}{\partial r}\right)^2 + 1}, \tag{1}$$

where ξ denotes the axial flame position, with respect to the flame base. Here, S_u and t are the laminar flame speed and time. Also, u and v are the axial and radial components of

flow velocity, and r denotes the radial coordinate. The linear dynamics of the flame can be analyzed by decomposing the variables into their mean and fluctuating parts and retaining only the linear terms in fluctuations. Assuming harmonic oscillations at an angular frequency, ω, for the fluctuating term yields the following equations for the mean and fluctuating variables:

$$\bar{u} = \bar{v}\frac{\mathrm{d}\bar{\xi}}{\mathrm{d}r} + \bar{S}_u\sqrt{\left(\frac{\mathrm{d}\bar{\xi}}{\mathrm{d}r}\right)^2 + 1}, \tag{2}$$

$$\begin{aligned} \mathrm{i}\omega\xi'(r) &= -u'(r) + \bar{v}\frac{\mathrm{d}\xi'}{\mathrm{d}r} + v'\frac{\mathrm{d}\bar{\xi}}{\mathrm{d}r} \\ &\quad + \bar{S}_u\frac{\left(\frac{\mathrm{d}\bar{\xi}}{\mathrm{d}r}\right)\frac{\mathrm{d}\xi'}{\mathrm{d}r}}{\sqrt{\left(\frac{\mathrm{d}\bar{\xi}}{\mathrm{d}r}\right)^2 + 1}} + S'_u\sqrt{\left(\frac{\mathrm{d}\bar{\xi}}{\mathrm{d}r}\right)^2 + 1}. \end{aligned} \tag{3}$$

The velocity fluctuation normal to the mean flame front [20] is denoted by $u'_n(r)$ and is given as:

$$u'_n = \left(u'(r) - v'(r)\frac{\mathrm{d}\bar{\xi}}{\mathrm{d}r}\right) \times \left[1 + \left(\frac{\mathrm{d}\bar{\xi}}{\mathrm{d}r}\right)^2\right]^{-\frac{1}{2}}. \tag{4}$$

The flow variables are normalized according to [20].

$$\begin{aligned} &(\hat{u}'_n, \hat{S}'_u, \hat{\bar{u}}, \hat{\bar{v}}, \hat{\bar{S}}_u) = (u'_n, S'_u, \bar{u}, \bar{v}, \bar{S}_u)/\bar{u}_0, \\ &(\hat{\xi}', \hat{\bar{\xi}}) = (\xi', \bar{\xi})/L_F, \qquad \hat{r} = \frac{r}{b-a}, \end{aligned} \tag{5}$$

where $L_F = \max(\xi(r))$ is mean flame length and $\bar{u}_0$ is mean flow speed at some reference point, such as at $r = (b-a)/2$ (see Figure 1). The normalized flame front equations are:

$$\hat{\bar{u}} = \frac{L_F}{b-a}\left[\hat{\bar{v}}\frac{\mathrm{d}\hat{\bar{\xi}}}{\mathrm{d}\hat{r}} + \hat{\bar{S}}_u\beta(\hat{r})\right], \tag{6}$$

$$\frac{\mathrm{d}\hat{\xi}'}{\mathrm{d}\hat{r}} + p(\hat{r})\hat{\xi}'(\hat{r}) = q(\hat{r}), \tag{7}$$

where:

$$\beta(\hat{r}) = \sqrt{\left(\frac{\mathrm{d}\hat{\bar{\xi}}}{\mathrm{d}\hat{r}}\right)^2 + \left(\frac{b-a}{L_F}\right)^2}, \tag{8a}$$

$$q(\hat{r}) = (\hat{u}'_n(\hat{r}) - \hat{S}'_u(\hat{r}))\frac{\beta(\hat{r})}{f(\hat{r})\hat{\bar{S}}_u}, \tag{8b}$$

$$p(\hat{r}) = \frac{(-\mathrm{i}\omega)(b-a)}{f(\hat{r})\hat{\bar{S}}_u u_0} = (-\mathrm{i})St\frac{|f|_m\bar{S}_{u,0}}{f(\hat{r})\hat{\bar{S}}_u u_0}, \tag{8c}$$

$$f(\hat{r}) = \frac{\frac{\mathrm{d}\hat{\bar{\xi}}}{\mathrm{d}\hat{r}}}{\beta(\hat{r})} + \frac{\hat{\bar{v}}(\hat{r})}{\hat{\bar{S}}_u(\hat{r})}. \tag{8d}$$

β in Eq. (8a) is the flame geometry factor and $\bar{v}$, the mean value of the radial component of the flow velocity, is assumed to be negligible. The Strouhal number is defined as the normalized frequency:

$$St = \frac{\omega(b-a)}{|f|_m\bar{S}_{u,0}}, \tag{9}$$

where $|f|_m = \max(|f(\hat{r})|)$ and $\bar{S}_{u,0}$ is a reference mean flame speed considered in the same way as in [20]. Following the assumption that the flame base remains anchored at its attachment point, the solution of Eq. (7) is given by:

$$\begin{aligned} \hat{\xi}'(\hat{r}) &= \int_{\frac{a}{b-a}}^{\hat{r}} \exp\left[\int_{\hat{r}}^{\eta} p(\tau)\mathrm{d}\tau\right] \\ &\quad \times \left[(\hat{u}'_n(\eta) - \hat{S}'_u(\eta))\frac{\beta(\eta)}{f(\eta)\hat{\bar{S}}_u(\eta)}\right]\mathrm{d}\eta. \end{aligned} \tag{10}$$

Fluctuation of the flame speed was assumed to have the following relation with the perturbation of equivalence ratio:

$$\hat{S}'_u(\eta) = \left.\frac{\mathrm{d}\hat{S}_u}{\mathrm{d}\phi}\right|_{\bar{\phi}}\phi'(\eta), \tag{11}$$

where ϕ is considered as the equivalence ratio, and $\bar{\phi}$ and ϕ' denote the mean and fluctuating parts of this equivalence ratio.

2.1. Calculation of flame transfer function

The total heat release response of the flame is considered in this section. Following Fleifil et al. [8], the global heat release rate of a flame is written as:

$$Q(t) = \int_{A_f}\rho S_u\Delta h_R\mathrm{d}A_f, \tag{12}$$

where A_f denotes the instantaneous flame surface area, and is obtained by integrating the axial flame displacement over the entire flame surface. Furthermore, ρ is the density of the unburned mixture, and Δh_R is the heat of reaction per unit mass of mixture. The differential element of the flame surface area ($\mathrm{d}A_f$) can be related to the flame position by the following relation:

$$\begin{aligned} \mathrm{d}A_f &= 2\pi r\left[\sqrt{1 + \left(\frac{\partial\xi}{\partial r}\right)^2}\right]\mathrm{d}r = \mathrm{d}\bar{A}_f + \mathrm{d}A'_f \\ &= 2\pi r\left[\sqrt{1 + \left(\frac{\partial\bar{\xi}}{\partial r}\right)^2}\right]\mathrm{d}r \\ &\quad + 2\pi r\left[\frac{\frac{\partial\bar{\xi}}{\partial r}\frac{\partial\xi'}{\partial r}}{\sqrt{1 + \left(\frac{\partial\bar{\xi}}{\partial r}\right)^2}}\right]\mathrm{d}r. \end{aligned} \tag{13}$$

As a consequence of the low Mach number assumption, the density of the reactive mixture is constant, i.e. the equivalence ratio perturbation occurs at constant density. Fluctuations in heat release can be decomposed into the separate contributions of flame speed, heat of reaction and flame surface area fluctuations, i.e:

$$Q' = Q'_{S_u} + Q'_{\Delta h_R} + Q'_{A_f}.$$

This relation can be rewritten as:

$$\begin{aligned} \frac{Q'}{\bar{Q}} &= \frac{\int\rho\Delta\bar{h}_R S'_u\mathrm{d}\bar{A}_f}{\int\rho\Delta\bar{h}_R\bar{S}_u\mathrm{d}\bar{A}_f} + \frac{\int\rho\bar{S}_u\Delta h'_R\mathrm{d}\bar{A}_f}{\int\rho\Delta\bar{h}_R\bar{S}_u\mathrm{d}\bar{A}_f} \\ &\quad + \frac{\int\rho\Delta\bar{h}_R\bar{S}_u\mathrm{d}A'_f}{\int\rho\Delta\bar{h}_R\bar{S}_u\mathrm{d}\bar{A}_f}. \end{aligned} \tag{14}$$

Cho and Lieuwen [20] have argued that the first term of Eq. (14) indicates that flame speed perturbation has a

direct effect on heat release fluctuation. This effect is due to fluctuations of the local consumption rate caused by the equivalence ratio perturbations, as indicated by Eq. (11). Eq. (10) indicates that there is also an indirect effect of flame speed perturbations on heat release fluctuations, which is accomplished through the generation of fluctuations in the flame surface area, as indicated by the last term of Eq. (14). On the other hand, velocity perturbation influences heat release fluctuations, due to the disturbances that are exerted on the instantaneous flame position and consequently on the flame surface area through the last term of Eq. (14). To see the above contributions, Eq. (14) is manipulated to be expressed in the following form [20]:

$$\frac{Q'}{\bar{Q}} = \frac{\int_{\frac{a}{b-a}}^{\frac{b}{b-a}} g(\hat{\bar{\xi}}(\hat{r}), St)\mathrm{d}\hat{r}}{\int_{\frac{a}{b-a}}^{\frac{b}{b-a}} \hat{\bar{S}}_u \Delta\bar{h}_R \beta(\hat{r})\hat{r}\mathrm{d}\hat{r}}, \tag{15}$$

where:

$$\begin{aligned} g(\hat{\bar{\xi}}(\hat{r}), St) = {} & \Delta\bar{h}_R \left(\frac{\partial\hat{\bar{\xi}}}{\partial\hat{r}}\right) \hat{r}\frac{\hat{u}'_n(\hat{r})}{f(\hat{r})} \\ & + \left[\left(\frac{\mathrm{d}(\Delta\bar{h}_R\hat{S}_u)}{\mathrm{d}\phi}\right)\bigg|_{\bar{\phi}} \beta(\hat{r}) \right. \\ & \left. - \frac{\Delta\bar{h}_R}{f(\hat{r})}\left(\frac{\partial\hat{\bar{\xi}}}{\partial\hat{r}}\right)\left(\frac{\mathrm{d}\hat{S}_u}{\mathrm{d}\phi}\right)\bigg|_{\bar{\phi}}\right] \hat{r}\phi'(\hat{r}) \\ & + (\mathrm{i}St)\left(\frac{\partial\hat{\bar{\xi}}}{\partial\hat{r}}\right)\frac{\Delta\bar{h}_R\hat{r}|f|_m\hat{\bar{S}}_{u,0}\hat{\xi}'(\hat{r})}{f(\hat{r})\beta(\hat{r})}. \end{aligned} \tag{16}$$

The three terms on the right-hand side of Eq. (16) describe the heat release response to coupled perturbations in flow velocity, equivalence ratio and flame displacement, respectively. The flame displacement perturbation is a function of flow velocity and equivalence ratio as shown in Eqs. (10) and (11).

2.2. V-flame response to the velocity and equivalence ratio perturbations

The prior section presented general results for the heat release response of a flame to equivalence ratio and velocity perturbations. In this section, we present explicit results for a V-shaped flame anchored on a central rod of radius (a), placed in a burner of radius (b), for a mixture of methane-air at atmospheric conditions with $P_0 = 1$ bar and $T_0 = 300$ K (see Figure 1). The mean value of the V-flame position is given by:

$$\begin{aligned} & \hat{\bar{\xi}}(\hat{r}) = \frac{\bar{\xi}}{L_F} = \frac{r-a}{b-a} = \hat{r} - \frac{a}{b-a}, \\ & \hat{r} = \frac{r}{b-a}; \qquad \frac{a}{b-a} \le \hat{r} \le \frac{b}{b-a}. \end{aligned} \tag{17}$$

Considering α as the flame angle, with respect to the mean flow direction, the expression for β (flame geometry factor) in Relation (8a) can be rewritten as:

$$\beta = \sqrt{1 + \left(\frac{b-a}{L_F}\right)^2} = \frac{1}{\cos\alpha}. \tag{18}$$

The Strouhal number is defined as the normalized frequency, $St = \beta\omega(b-a)/\bar{S}_{u,0} = (\beta^2\omega L_F)/\bar{u}$. In this description, $\bar{S}_{u,0}$, which is the reference mean flame speed, can be replaced by $\bar{S}_u$, since it is assumed that $\bar{S}_u$ is spatially uniform (see Eq. (6)). The equivalence ratio disturbance is assumed to be convected by the mean flow as given below:

$$\begin{aligned} \phi'(\eta) &= \phi'_b \exp\left[\frac{\mathrm{i}\omega\bar{\xi}(\eta)}{\bar{u}(\eta)}\right] \\ &= \phi'_b \exp\left[\frac{\mathrm{i}St}{\beta^2}\left(\eta - \frac{a}{b-a}\right)\right] \end{aligned} \tag{19}$$

where ϕ'_b denotes the value of the perturbation at the base of the flame. We assume that the velocity perturbation consists of a uniform and an axially convected component. So, the velocity perturbation, $\hat{u}'_n(\hat{r})$, in the first term of Eq. (16) is given by:

$$\hat{u}'_n(\hat{r}) = \hat{u}'_{n,uni} + \hat{u}'_{n,cv} \exp\left[\frac{\mathrm{i}St}{\beta^2}\left(\hat{r} - \frac{a}{b-a}\right)\right], \tag{20}$$

where $\hat{u}'_{n,uni}$ and $\hat{u}'_{n,cv}$ denote uniform and convected velocity perturbations, respectively. The uniform velocity perturbations represent the disturbance of a flame by a long wavelength acoustic perturbation, as shown by Fleifil et al. [8]. However, based on the studies of Schuller et al. [12], the axially convected velocity perturbations represent the propagation of a vortical disturbance along the flame. These vortical disturbances are usually generated because of the upstream velocity perturbations, due either to fluid mechanical phenomena, such as vortex shedding off a flame holder or to interaction of the combustor with upstream or downstream hardware [14]. Both uniform and convected velocity perturbations are considered to improve the theoretical predictions of the flame transfer function at higher frequencies.

Substituting Eq. (19) into Eq. (11) and the obtained result plus Eq. (20) into Eq. (10) and subsequently substituting the obtained result from Eq. (10) into Eq. (15) yields the following expression for the flame transfer functions:

$$\frac{Q'}{\bar{Q}} = \left(\frac{\hat{u}'_{n,uni}}{\hat{\bar{S}}_u}\right) F_{u,uni} + \left(\frac{\hat{u}'_{n,cv}}{\hat{\bar{S}}_u}\right) F_{u,cv} + \left(\frac{\phi'_b}{\bar{\phi}}\right) F_\phi, \tag{21}$$

where $F_{u,uni}$ represents the flame response to the uniform acoustic velocity perturbations and $F_{u,cv}$ expresses the flame response to the axially convected velocity perturbations, due to the propagation of vortical disturbances along the flame. The flame response to the equivalence ratio perturbations is represented by F_ϕ. These transfer functions can be rewritten as the following relations:

$$\begin{aligned} F_{u,uni} &= \left(\frac{Q'_{u,uni}}{\bar{Q}}\right)\left(\frac{\hat{u}'_{n,uni}}{\hat{\bar{S}}_u}\right)^{-1} \\ &= \frac{2}{St^2}\frac{b-a}{b+a}\left\{(\mathrm{i}St)\left[\frac{a}{b-a} - \frac{b}{b-a}\exp(\mathrm{i}St)\right] \right. \\ &\quad \left. + \exp(\mathrm{i}St) - 1\right\}, \end{aligned} \tag{22}$$

$$\begin{aligned} F_{u,cv} &= \left(\frac{Q'_{u,cv}}{\bar{Q}}\right)\left(\frac{\hat{u}'_{n,cv}}{\hat{\bar{S}}_u}\right)^{-1} = \frac{-2\beta^2}{St^2(\beta^2-1)}\frac{b-a}{b+a} \\ &\quad \times \left\{(\mathrm{i}St)\frac{b}{b-a}\left[\exp(\mathrm{i}St) - \exp\left(\frac{\mathrm{i}St}{\beta^2}\right)\right] \right. \\ &\quad \left. + [1 - \exp(\mathrm{i}St)] + \beta^2\left[\exp\left(\frac{\mathrm{i}St}{\beta^2}\right) - 1\right]\right\}, \end{aligned} \tag{23}$$

$$F_\phi = \left(\frac{Q'_\phi}{\bar{Q}}\right)\left(\frac{\phi'_b}{\bar{\phi}}\right)^{-1} = F_H + F_S = F_H + (F_{S,\mathrm{dir}} + F_A). \quad (24)$$

Eq. (24) indicates that the equivalence ratio perturbations exert two distinct effects on heat release. The first term, F_H, is due to perturbations in the heat of the reaction and the second term, F_S, is due to perturbations in flame speed. Furthermore, the flame response to the flame speed perturbations can be divided into the response due to the direct effect of equivalence ratio perturbations on flame speed, $F_{S,\mathrm{dir}}$, and the indirect effect of the equivalence ratio perturbation on the flame surface area, F_A, due to the perturbations of flame speed. These transfer functions are given as:

$$F_H = \left.\frac{\mathrm{d}(\Delta h_R/\Delta\bar{h}_R)}{\mathrm{d}(\phi/\bar{\phi})}\right|_{\bar{\phi}} \frac{2\beta^2}{St^2}\frac{b-a}{b+a} \times \left\{(\mathrm{i}St)\left[\frac{a}{b-a} - \frac{b}{b-a}\exp\left(\frac{\mathrm{i}St}{\beta^2}\right)\right] + \beta^2\left[\exp\left(\frac{\mathrm{i}St}{\beta^2}\right) - 1\right]\right\}, \quad (25)$$

$$F_{S,\mathrm{dir}} = \left.\frac{\mathrm{d}(S_u/\bar{S}_u)}{\mathrm{d}(\phi/\bar{\phi})}\right|_{\bar{\phi}} \frac{2\beta^2}{St^2}\frac{b-a}{b+a} \times \left\{(\mathrm{i}St)\left[\frac{a}{b-a} - \frac{b}{b-a}\exp\left(\frac{\mathrm{i}St}{\beta^2}\right)\right] + \beta^2\left[\exp\left(\frac{\mathrm{i}St}{\beta^2}\right) - 1\right]\right\}, \quad (26)$$

$$F_A = \left.\frac{\mathrm{d}(S_u/\bar{S}_u)}{\mathrm{d}(\phi/\bar{\phi})}\right|_{\bar{\phi}} \frac{2\beta^2}{St^2(1-\beta^2)}\frac{b-a}{b+a} \times \left\{(\mathrm{i}St)\frac{b}{b-a}\left[\exp\left(\frac{\mathrm{i}St}{\beta^2}\right) - \exp(\mathrm{i}St)\right] + [\exp(\mathrm{i}St) - 1] - \beta^2\left[\exp\left(\frac{\mathrm{i}St}{\beta^2}\right) - 1\right]\right\}. \quad (27)$$

The above equations state that $F_{u,cv}$ and F_ϕ are functions of Strouhal number, flame angle, and rod and burner radii. In contrast, $F_{u,uni}$ is only a function of the Strouhal number and burner dimensions, due to the assumption of spatially uniform acoustic velocity perturbations.

Regarding Eqs. (25)–(27), to determine the dependency of flame speed and heat of reaction perturbations upon the equivalence ratio fluctuations, explicit relations should be presented. In order to do this, a quasi-steady relationship between equivalence ratio and flame speed (or heat of reaction) is assumed. In other words, $d(S_u/\bar{S}_u)/d(\phi/\bar{\phi})$ and $d(\Delta h_R/\Delta\bar{h}_R)/d(\phi/\bar{\phi})$ are considered to be independent of frequency. For a mixture of methane-air at atmospheric condition, the following correlation can be used to quantify the dependence of the heat of reaction and flame speed upon the equivalence ratio [25]:

$$S_u(\phi) = A\phi^B \mathrm{e}^{-C(\phi-D)^2} \quad (\mathrm{m/s}), \quad (28)$$

where $A = 0.6079$, $B = -2.554$, $C = 7.31$ and $D = 1.230$.

$$\Delta h_R(\phi) = \frac{2.9125 \times 10^6 \min(1,\phi)}{1 + 0.05825\phi} \ (\mathrm{J/kg}). \quad (29)$$

3. Results and discussion

A V-flame anchored on a thin central rod is considered. This condition corresponds to the limiting case of a large burner radii (b) compared to the radius of central rod ($b/a \gg 1$). The variation of the flame transfer function, with respect to the Strouhal number, is presented. Figure 2 shows the magnitude of F_ϕ, F_S, F_H and $F_{u,uni}$. It indicates that $F_{u,uni}$ and F_H have an almost similar behavior, especially at higher excitation frequencies. F_H decreases monotonically from its maximum response at $St = 0$, whereas F_S increases from its trivial value at $St = 0$ and reaches a maximum of about 1.7 around St ∼5. As a consequence, at low Strouhal numbers ($St \sim 0$), the heat of reaction has a dominant contribution to F_ϕ.

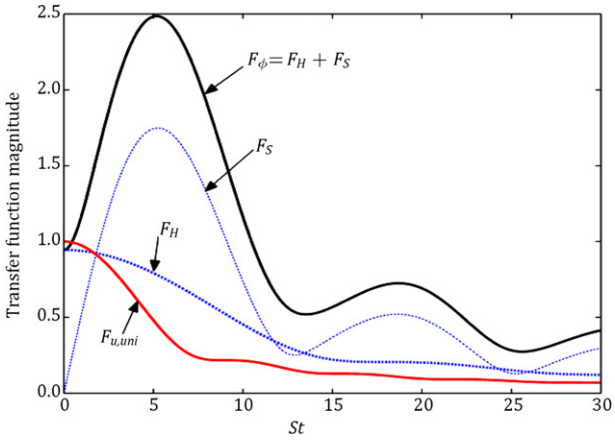

Figure 2: Dependence of the magnitude of V-flame transfer function upon Strouhal number ($L_F/(b-a) = 1, (\alpha = 45°)$ and $\bar{\phi} = 1$).

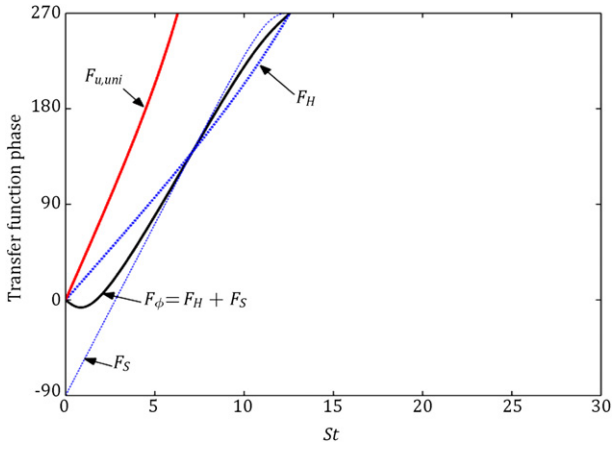

Figure 3: Dependence of the phase of V-flame transfer function upon Strouhal number ($L_F/(b-a) = 1, (\alpha = 45°)$ and $\bar{\phi} = 1$).

The variations in phase of F_ϕ, F_S, F_H and $F_{u,uni}$ are plotted in Figure 3. The phases of all transfer functions increase almost linearly with St, whereas for the case of $F_{u,uni}$, the phase increases with a higher slope than those of other transfer functions. This is because the required time for acoustic velocity fluctuations to reach the flame surface is different from that of the disturbances of the equivalence ratio.

Considering Figures 4 and 5, the trivial value of F_S, around $St \sim 0$, could be due to the cancellation of the contributions from $F_{S,\mathrm{dir}}$ and F_A, which have equal magnitudes, but opposite phases at lower limits of Strouhal number. This behavior is the same as that of conical flames at the limit of zero excitation frequencies [20]. In other words, flame speed and flame area, in the case of a V-flame, fluctuate with the opposite phase at the limit of zero excitation frequency, with the same behavior as that of the conical flame [20]. This is because, in this range of

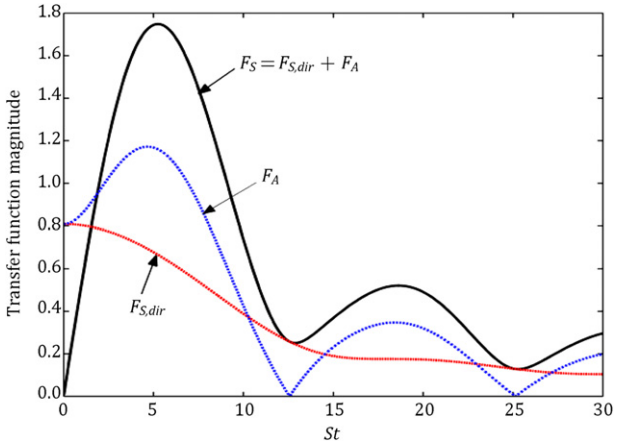

Figure 4: Magnitude of V-flame transfer function due to direct flame speed, $F_{S,\mathrm{dir}}$, and flame area, F_A, fluctuation ($L_F/(b-a) = 1$, ($\alpha = 45°$) and $\bar{\phi} = 1$).

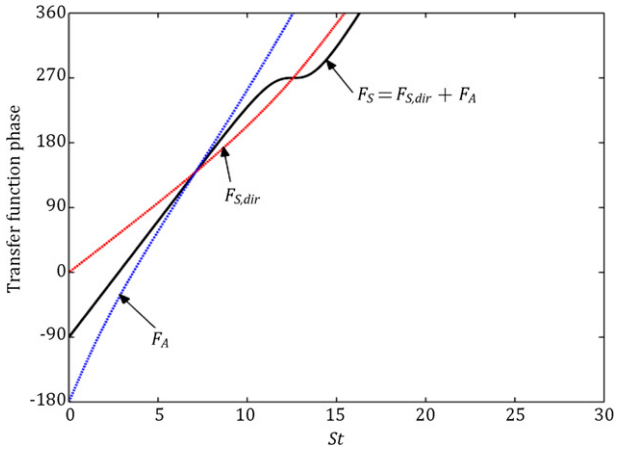

Figure 5: Phase of V-flame transfer function due to direct flame speed, $F_{S,\mathrm{dir}}$, and flame area, F_A, fluctuation ($L_F/(b-a) = 1$, ($\alpha = 45°$) and $\bar{\phi} = 1$).

frequencies ($St \sim 0$), the flame length remains much less than the wavelength of convective disturbances, such as equivalence ratio fluctuations. As a consequence, flame response would be independent of flame configuration. In other words, both the V-flame and the conical flame may exhibit a similar response at the limit of zero excitation frequency, around $St \sim 0$. To gain a better understanding of the flame's zero response to flame speed perturbation, around $St \sim 0$, it should be considered that the long time scale perturbations can influence the flame's local consumption rate, whereas the resultant heat release perturbation would be exactly balanced by the resultant variations in flame area.

Considering Figure 4, F_S increases with Strouhal number from zero because the phase difference between the terms $F_{S,\mathrm{dir}}$ and F_A decreases with Strouhal number until the point where this phase difference becomes negligible, around $St \sim 8$. As such, these two terms add constructively to enhance the combined flame speed term, F_S. F_S reaches a global maximum at $St \sim 5$, where the two terms, $F_{S,\mathrm{dir}}$ and F_A, add together in the most constructive manner and reinforce each other. As the Strouhal number increases further, F_S decreases in an oscillatory pattern, due to the alternating phase difference between $F_{S,\mathrm{dir}}$ and F_A and their decreasing magnitudes.

It is noteworthy that the magnitude of F_A vanishes at some values of St, such as St ∼12.5, 25. This might be due to the propagation of equivalence-ratio oscillations, which exert spatial variations along the flame front. This can lead to generation of heat-release disturbances at different points of the flame that are out of phase with each other. Consequently, in certain frequencies, these local heat-release disturbances can destructively cancel each other out, so that the resulting response equals zero.

The magnitude of F_ϕ in Figure 2 also increases until $St \sim 5$, with the same behavior as F_S, and decreases in an oscillatory manner with further increasing St, due to the alternating magnitudes of F_H and F_S. Actually, the behavior of F_s is complex, due to the contribution of the flame's position and the resultant variation of flame surface area. In addition, the contributions from perturbations in $F_{s,\mathrm{dir}}$ and F_A constructively and destructively interfere, depending on the frequency of oscillations. The oscillatory pattern of F_s at higher Strouhal numbers is due to the constructive and destructive contributions of $F_{s,\mathrm{dir}}$ and F_A.

It should also be noted that the trend of variation in magnitude of $F_{u,\mathrm{uni}}$ upon Strouhal number in the case of a V-flame (see Figure 2) is similar to that of the conical flame obtained in previous related studies [12,20]. This is due to the identical expressions that are obtained for calculations of this magnitude in both flame configurations. At the limits of large burner radii (b) compared to the radius of the central rod, considering Eq. (22) in the present study, together with Eq. (31) in the study of Cho and Lieuwen [20] or Eq. (22) in Ref. [12], the calculated magnitude of $F_{u,\mathrm{uni}}$ can be written as follows:

$$|F_{u,\mathrm{uni}}| = \frac{2}{St^2}\sqrt{2 + St^2 - 2\cos(St) - 2St\sin(St)}. \tag{30}$$

It is also worth noting that the obtained Relations (22) and (23) for $F_{u,\mathrm{uni}}$ and $F_{u,cv}$ in the present study, respectively, coincide with Expressions (30) and (33) presented in [12], by using a different modeling approach. On the other hand, variation in the phase of $F_{u,\mathrm{uni}}$ for the case of a V-flame exhibits different characteristics from those of the conical flame [12,20]. The phase response of the conical flame (phase of $F_{u,\mathrm{uni}}$) starts from zero at $St = 0$, whereas it increases to and oscillates around 90° for the higher ranges of Strouhal number [20]. On the contrary, in the case of V-flames, the phase evolves quasi-linearly with Strouhal number. This indicates that the fluctuations require a certain time to reach the flame surface in the case of V-flames. This result was also experimentally confirmed by a previous related study [16].

Variations in magnitude of F_ϕ and F_H, versus the flame Strouhal number, in the case of V-flames, are compared with those of conical flames in Figure 6. Results of conical flame response are obtained from the study of Cho and Lieuwen [20]. The responses of V-flame and conical flame, with the same flame length, to disturbances of heat of reaction exhibit a similar trend for the whole range of frequency. This is due to the identical relations obtained for calculation of the magnitude of F_H in both flame configurations. This expression is given as:

$$|F_H| = \left.\frac{\mathrm{d}(\Delta h_R/\Delta\bar{h}_R)}{\mathrm{d}(\phi/\bar{\phi})}\right|_{\bar{\phi}} \frac{2\beta^4}{St^2}\left\{2 + \left(\frac{St}{\beta^2}\right)^2 - 2\cos\left(\frac{St}{\beta^2}\right) - 2\left(\frac{St}{\beta^2}\right)\sin\left(\frac{St}{\beta^2}\right)\right\}^{0.5}. \tag{31}$$

On the contrary, the phase of F_H for the conical flame starts from zero, at $St = 0$, and tends to be saturated around 90° for higher ranges of Strouhal number [20]. However, the phase of F_H, in the

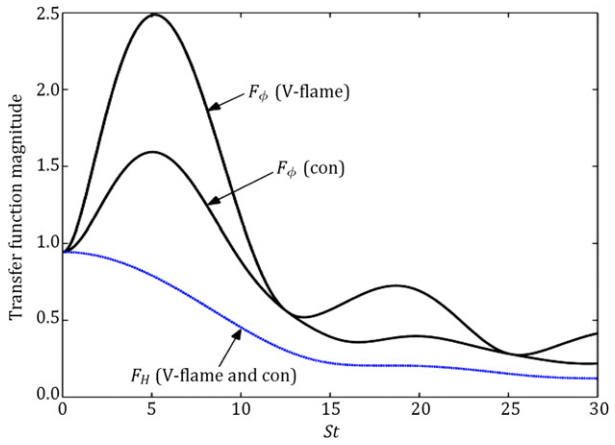

Figure 6: Magnitude of the flame response to equivalence ratio perturbations for a conical [20] and V-flame ($\alpha = 45^\circ$ and $\bar{\phi} = 1$).

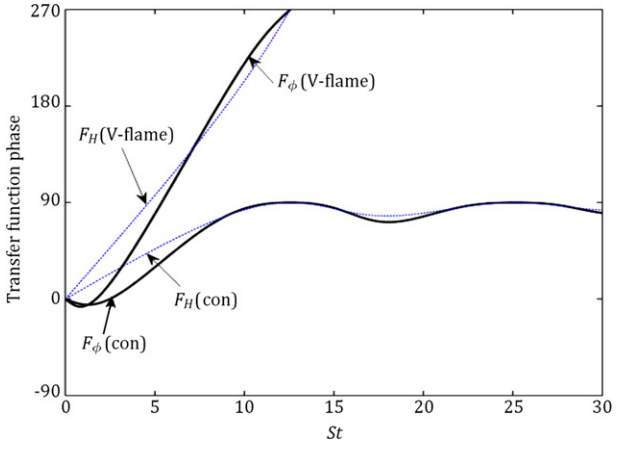

Figure 7: Phase of the flame response to equivalence ratio perturbations for a conical [20] and V-flame ($\alpha = 45^\circ$ and $\bar{\phi} = 1$).

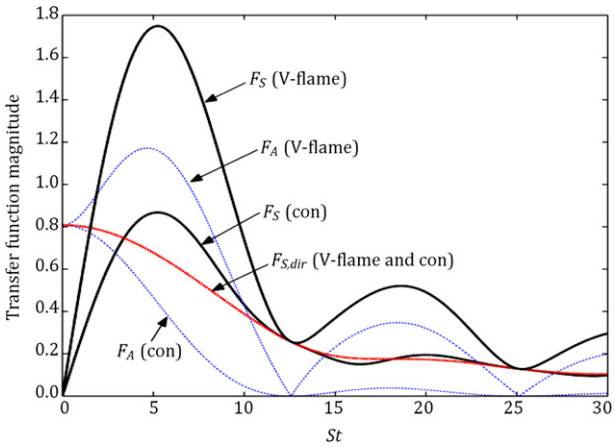

Figure 8: Magnitude of the flame speed transfer function versus Strouhal number for conical [20] and V-shaped flame ($\alpha = 45^\circ$ and $\bar{\phi} = 1$).

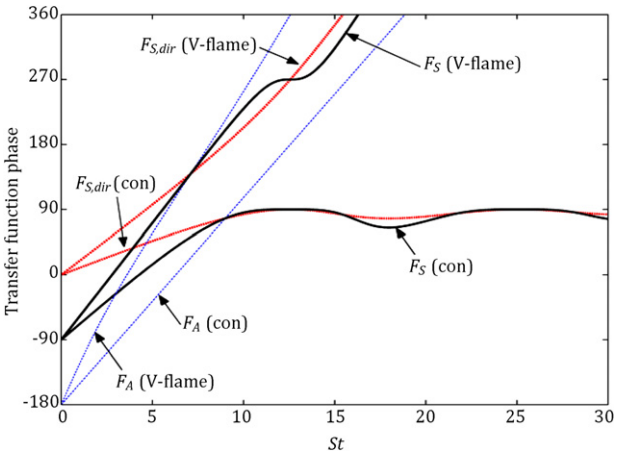

Figure 9: Phase of the flame speed transfer function versus Strouhal number for conical [20] and V-shaped flame ($\alpha = 45^\circ$ and $\bar{\phi} = 1$).

case of V-flames, evolves quasi-linearly, with $\Phi \sim St/\beta^2$, by an increase in frequency (See Figure 7). Here, Φ denotes the phase of flame transfer function. Figure 6 also indicates that F_ϕ, in the case of V-flames, increases with a higher overshoot compared to the conical flame. As the Strouhal number increases further, F_ϕ decreases in a stronger oscillatory pattern, in the case of the V-flame, with higher amplitude in each cycle of oscillation. F_ϕ reaches a global maximum around $St \sim 5$ for both flame configurations.

Figures 8 and 9 plot the dependence of the flame transfer function upon Strouhal number for two flame configurations. It is shown that the magnitude of F_S for the V-flame increases with Strouhal number to a higher value than that of the conical flame. The magnitude of F_S for the V-flame increases to values of greater than unity, at a certain range of frequencies, due to the constructive interference between $F_{s,\mathrm{dir}}$ and F_A. As the Strouhal number increases further, F_S decreases in a stronger oscillatory pattern, in the case of the V-flame. For both cases, $F_{s,\mathrm{dir}}$ exhibits identical behavior, which is due to the similar relations obtained for calculation of the magnitude of $F_{s,\mathrm{dir}}$ in both flame configurations. The higher value of F_S for the V-flame is due to the stronger contribution of F_A, compared with that of the conical flame. The higher amount of F_A, in the case of the V-flame, is because of the relatively stronger and faster variation of its surface, due to propagation of the equivalence ratio perturbation along the flame. This was also proposed by another related experimental study [15]. Hereafter, $F_{s,\mathrm{dir}}$, for conical and V-flames, will be denoted by $F_{s,\mathrm{dir}}$ (Con) and $F_{s,\mathrm{dir}}$ (V-flame), respectively. The phase of $F_{s,\mathrm{dir}}$ (Con) exhibits a saturation behavior at $\pi/2$ (around 90°) for large Strouhal numbers, whereas the phase of $F_{s,\mathrm{dir}}$ (V-flame) increases linearly with $\Phi \sim St/\beta^2$ (for the flame with $\alpha = 45^\circ$, this phase would be $\Phi \sim St/2$), at the higher ranges of Strouhal number (see Figure 9). It is also interesting to note that the phase of F_s (Con) exhibits phase saturation at $\pi/2$ for large Strouhal numbers. However, the phase of F_s (V-flame) increases in a quasi-linear manner around $\Phi \sim St/2^*[(\beta^2+1)/\beta^2]$ (for the flame with $\alpha = 45^\circ$, this value would be $\Phi \sim 3St/4$).

Figures 10–13 indicate the effects of the ratio of flame length to the burner gap, $L_F/(b-a)$, on the flame transfer function. These figures are shown for some values of $L_F/(b-a)$ such as 0.3, 1, 3, and 20 (corresponding to $\alpha \sim 73^\circ, 45^\circ, 18^\circ$ and 3°, respectively). The above-mentioned values were chosen in order to compare the results with those of the conical flames obtained from the study of Cho and Lieuwen [20], considering $\bar{\phi} = 0.6$. As illustrated in Figures 10 and 12, the behavior of the magnitude of transfer functions for V-flames and conical flames are independent of the value of $L_F/(b-a)$ at the lower limit of excitation frequency, around $St \sim 0$. This behavior, in the case of conical flames, was also reported previously in [20].

This flame's behavior could be explained by considering the definition of St as the ratio of flame length to the wavelength

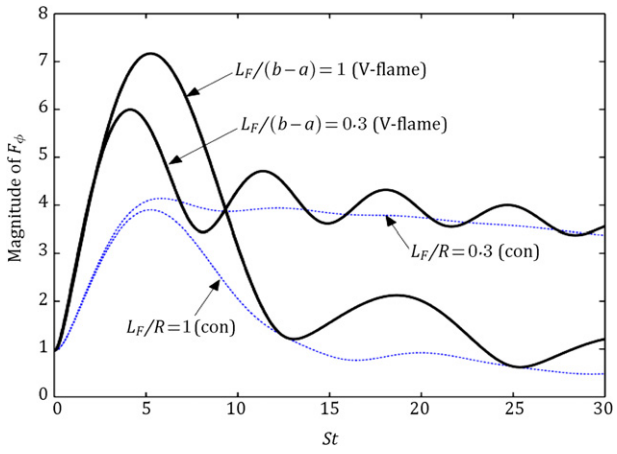

Figure 10: Magnitude of the flame transfer function versus Strouhal number for conical [20] and V-shaped flame ($L_F/(b-a) = 0.3, 1$ ($\alpha = 73°, 45°$) and $\bar{\phi} = 0.6$).

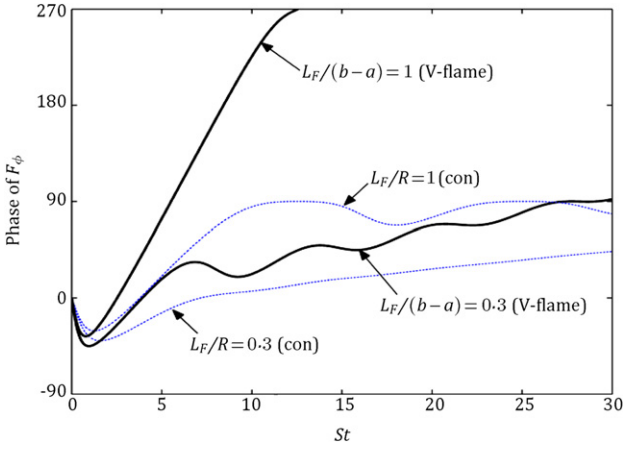

Figure 11: Phase of the flame transfer function versus Strouhal number for conical [20] and V-shaped flame ($L_F/(b-a) = 0.3, 1$ ($\alpha = 73°, 45°$) and $\bar{\phi} = 0.6$).

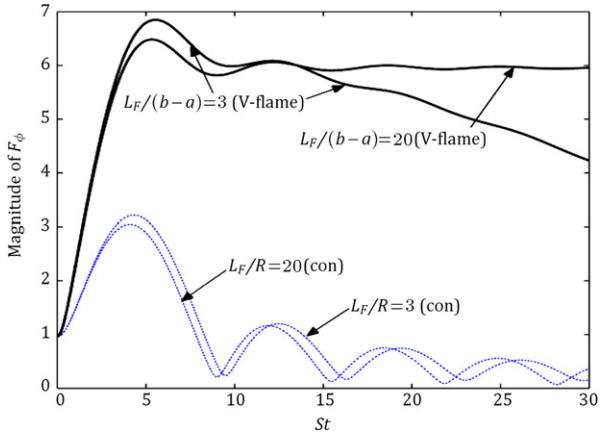

Figure 12: Magnitude of the flame transfer function for conical [20] and V-shaped flame ($L_F/(b-a) = 3, 20$ ($\alpha = 18°, 3°$) and $\bar{\phi} = 0.6$).

of convective disturbances. For the lower range of excitation frequency (i.e., $St \sim 0$), the flame length remains much less than a convective wavelength. In consequence, the flame would not be sensitive to propagation of convective perturbations, and

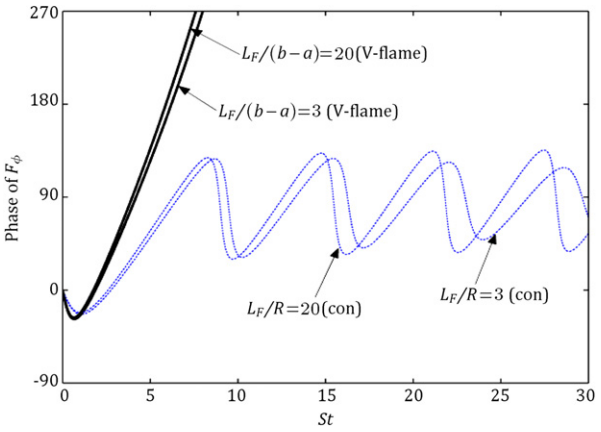

Figure 13: Phase of the flame transfer function for conical [20] and V-shaped flame ($L_F/(b-a) = 3, 20$ ($\alpha = 18°, 3°$) and $\bar{\phi} = 0.6$).

the flame front will appear as a discontinuity to the convective wave. In other words, for frequencies around $St \sim 0$, the flame response would be independent of flame length.

An increase in Strouhal number to the higher values leads to an increase in F_ϕ to its maximum of about 6 to 7, around $St \sim 5$, for the case of V-flames. With further increase of St, the flame transfer function decreases in an oscillatory pattern for the cases of $L_F/(b-a) = 0.3, 1$. It is indicated in Figure 10 that the maximum value of the transfer function is higher for the longer V-flame, with $L_F/(b-a) = 1$. This result is in contrast to the obtained results for the case of the conical flame. In conical flames, the maximum value of flame response was reported to be higher for shorter flames [20].

It should be noted that for longer V-flames, the flame length may be of the same order or longer than a convective wavelength. Thus, a convected disturbance, such as an equivalence-ratio oscillation, may lead to local heat release perturbations along the flame front, which could simply be added to generate a high value of flame response at a broad range of excitation frequencies. As a consequence, long V-flames are quite sensitive to any low frequency perturbations and keep their high value of response over a large range of frequencies.

Short V-flames ($L_F/(b-a) = 0.3, 1$), on the other hand, exhibit more oscillatory patterns in the gain of their response relative to the conical flames (see Figure 10). These oscillations might be due to the constructive and destructive interference between the contributions of $F_{S,\text{dir}}$ and F_A. However, the oscillations vanish at higher Strouhal numbers. The phase results in Figures 11 and 13 also show a more oscillatory pattern for shorter V-flames. For higher Strouhal numbers, the phase response of all V-flames oscillates around a certain value of Φ, as given in Eq. (32). The results suggest that the phase behavior, for larger values of excitation frequency, depends on the flame angle and mean equivalence ratio ($\bar{\phi}$).

$$\Phi = \tan^{-1}\left[\frac{\Psi\cos\left(\frac{St}{\beta^2}\right) - \Gamma\cos(St)}{-\Psi\sin\left(\frac{St}{\beta^2}\right) + \Gamma\sin(St)}\right], \tag{32}$$

where:

$$\Psi = -\frac{\mathrm{d}(\Delta h_R/\Delta\bar{h}_R)}{\mathrm{d}(\phi/\bar{\phi})}\bigg|_{\bar{\phi}} + \left(\frac{\beta^2}{1-\beta^2}\right)\frac{\mathrm{d}(S_u/\bar{S}_u)}{\mathrm{d}(\phi/\bar{\phi})}\bigg|_{\bar{\phi}},$$

$$\Gamma = \left(\frac{1}{1-\beta^2}\right)\frac{\mathrm{d}(S_u/\bar{S}_u)}{\mathrm{d}(\phi/\bar{\phi})}\bigg|_{\bar{\phi}}. \tag{33}$$

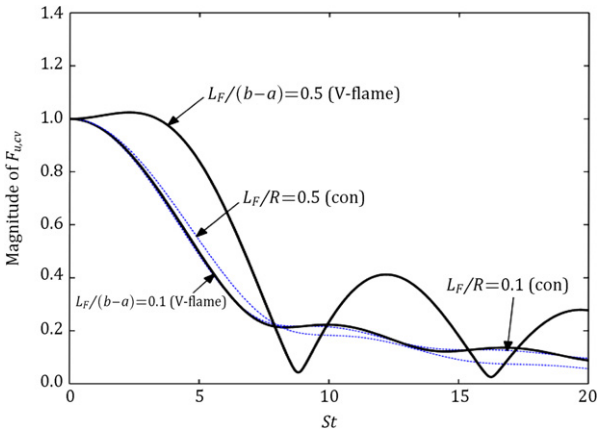

Figure 14: Magnitude of the flame response to convected velocity perturbations for a conical [20] and V-shaped flame ($L_F/(b-a) = 0.1, 0.5$ ($\alpha = 84°, 63°$) and $\bar{\phi} = 1$).

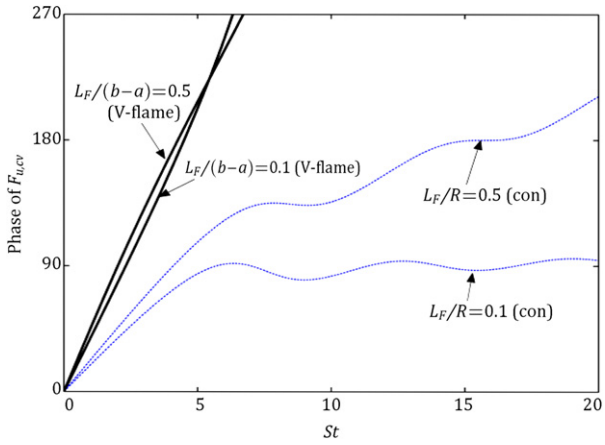

Figure 15: Phase of the flame response to convected velocity perturbations for a conical [20] and V-shaped flame ($L_F/(b-a) = 0.1, 0.5$ ($\alpha = 84°, 63°$) and $\bar{\phi} = 1$).

The dependence of $F_{u,cv}$ upon St for various values of $L_F/(b-a)$ are shown in Figures 14–17. The results of the magnitude and phase of $F_{u,cv}$ for three flame angles of $\alpha = 15°, 50°$, and $88°$ were similar to those obtained in the study of Schuller et al. [12] (not shown here). To investigate the various features of V-flames and conical flames, the results of $F_{u,cv}$, for V-flames with angles of $\alpha = 11°, 45°, 63°$ and $84°$, are compared with those of conical flames obtained in the study of Cho and Lieuwen [20].

It is important to note that the response of conical flames to convected velocity perturbations has a value of unity at zero frequency and decays with frequency, as shown in Figures 14 and 16. In contrast, for long V-flames with $L_F/(b-a) > 0.5$, the magnitude of $F_{u,cv}$ exceeds unity and shows an oscillatory behavior at a certain range of frequency. This increase in gain to values of greater than unity for long V-flames was also predicted previously by Schuller et al. [12]. For longer V-flames ($L_F/(b-a) \geq 1$), the range of frequency at which the gain keeps a value higher than unity increases. This indicates that the longer V-flames are more sensitive to axially convected velocity perturbations. For $L_F/(b-a) = 5$ ($\alpha = 11°$), the V-flame response shows a resonance-like behavior, where it does not decrease with St, but tends towards a constant value of two (see Figure 16). This case may correspond to the coincidence of flame front and convected velocity disturbances. For long V-flames (with $\alpha < 45°$), the phase response (see Figure 17) increases linearly, around $\Phi \sim St/2^*[(\beta^2+1)/\beta^2]$ for large values of Strouhal number.

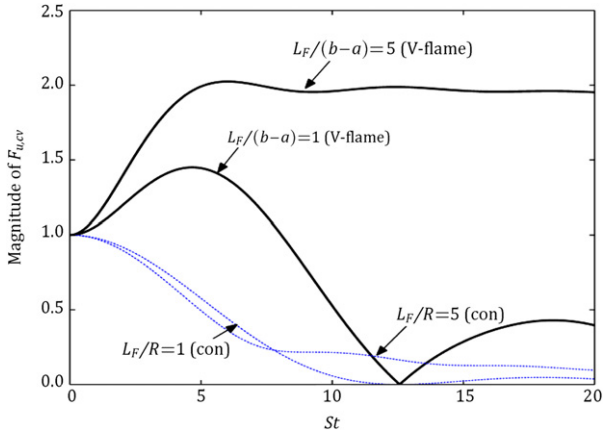

Figure 16: Magnitude of the flame response to convected velocity perturbations for a conical [20] and V-shaped flame ($L_F/(b-a) = 1, 5$ ($\alpha = 45°, 11°$) and $\bar{\phi} = 1$).

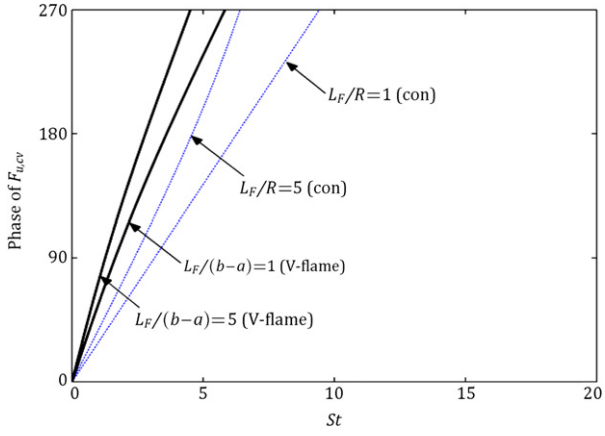

Figure 17: Phase of the flame response to convected velocity perturbations for a conical [20] and V-shaped flame ($L_F/(b-a) = 1, 5$ ($\alpha = 45°, 11°$) and $\bar{\phi} = 1$).

4. Conclusion remarks

The objective of the present study was to examine the response of a premixed V-flame to the upstream velocity and equivalence ratio oscillations, and to compare these results with those of a conical flame. The flame-speed disturbances were considered to influence the heat-release perturbations by generating perturbations in both flame area and consumption rate.

The results show that in the case of V-flames, the phase response evolves quasi-linearly with Strouhal number, which was also confirmed by a previous related study [16]. This indicates that the fluctuations require a certain time to reach the flame surface. V-flames are more sensitive to the convected velocity and equivalence ratio perturbations than conical flames, and by an increase in flame length, this susceptibility enhances. For certain long V-flames, the response of the transfer function to convected velocity perturbations exhibits a resonant-like behavior. This might be due to the coincidence of the flame front and the convected velocity perturbation.

The higher value of the overall response of the V-flame to equivalence ratio perturbations is due to the stronger and faster variation of its surface during propagation of these disturbances along the flame. In other words, the contribution of flame tip displacement on the fluctuations of the flame surface, in the case of the V-flame, is stronger than that of the conical flame. As a consequence, conical flames have a limited degree of freedom and are relatively more stable to the upstream flow perturbations. The results suggest that V-flames are able to amplify flow perturbations, such as equivalence ratio disturbances, at certain frequency ranges, indicating that they are more susceptible to combustion instabilities than conical flames.

References

[1] Zimont, V.L. "Theory of turbulent combustion of a homogeneous fuel mixture at high Reynolds numbers", *Combustion, Explosion, and Shock Waves*, 15, pp. 305–311 (1979).
[2] Broda, J.C., Seo, S., Santoro, R.J., Shirhattikar, G. and Yang, V. "An experimental study of combustion dynamics of a premixed swirl injector", *Proceedings of the Combustion Institute*, 27, pp. 1849–1856 (1998).
[3] Candel, S. "Combustion dynamics and control: progress and challenges", *Proceedings of the Combustion Institute*, 29, pp. 1–28 (2002).
[4] Dowling, A.P. and Stow, S.R. "Acoustic analysis of gas turbine combustors", *Journal of Propulsion and Power*, 19(5), pp. 751–764 (2003).
[5] Ducruix, S., Schuller, T., Durox, D. and Candel, S. "Combustion dynamics and instabilities: elementary coupling and driving mechanisms", *Journal of Propulsion and Power*, 19(5), pp. 722–734 (2003).
[6] Bellows, B.D. and Lieuwen, T. "Nonlinear response of a premixed combustor to forced acoustic oscillations", AIAA 2004-0455 (2004).
[7] Lieuwen, T. "Modeling premixed combustion-acoustic wave interactions: a review", *Journal of Propulsion and Power*, 19(5), pp. 765–781 (2003).
[8] Fleifil, M., Annaswamy, A.M., Ghoniem, Z. and Ghoniem, A.F. "Response of a laminar premixed flame to flow oscillations: a kinematic model and thermo-acoustic result", *Combustion and Flame*, 106(4), pp. 487–510 (1996).
[9] Ducruix, S., Durox, D. and Candel, S. "Theoretical and experimental determinations of the transfer function of a laminar premixed flame", *Proceedings of the Combustion Institute*, 28, pp. 765–773 (2000).
[10] Lieuwen, T., Torres, H., Johnson, C. and Zinn, B.T. "A mechanism of combustion instability in lean premixed gas turbine combustors", *Journal of Engineering for Gas Turbines and Power*, 123, pp. 182–190 (2001).
[11] Schuller, T., Ducruix, S., Durox, D. and Candel, S. "Modeling tools for the prediction of premixed flame transfer functions", *Proceedings of the Combustion Institute*, 29, pp. 107–113 (2002).
[12] Schuller, T., Durox, D. and Candel, S. "A unified model for the prediction of laminar flame transfer functions: comparisons between conical and V-flame dynamics", *Combustion and Flame*, 134, pp. 21–34 (2003).
[13] Lieuwen, T. "Nonlinear kinematic response of premixed flames to harmonic velocity disturbances", *Proceedings of the Combustion Institute*, 30, pp. 1725–1732 (2005).
[14] Chaparro, A., Landry, E. and Cetegen, B.M. "Transfer function characteristics of bluff-body stabilized, conical V-shaped premixed turbulent propane-air flames", *Combustion and Flame*, 145, pp. 290–299 (2006).
[15] Schuller, T., Durox, D. and Candel, S. "Self-induced combustion oscillations of laminar premixed flames stabilized on annular burners", *Combustion and Flame*, 135, pp. 525–537 (2003).
[16] Durox, D., Schuller, T., Noiray, N. and Candel, S. "Experimental analysis of nonlinear flame transfer functions for different flame geometries", *Proceedings of the Combustion Institute*, 32, pp. 1391–1398 (2009).
[17] Baillot, F., Bourehla, A. and Durox, D. "The characteristic method and cusped flame fronts", *Combustion Science and Technology*, 112, pp. 327–350 (1996).
[18] Ducruix, S., Durox, D. and Candel, S. "Flow velocity in a flame submitted to acoustic modulation", *18th International Colloquium on Dynamics of Explosion and Reactive Systems*, Seattle, WA (2001).
[19] Bloxsidge, G.J., Dowling, A.P. and Langhorne, P.J. "Reheat buzz: an acoustically coupled combustion instability. Part 2. Theory", *Journal of Fluid Mechanics*, 193, pp. 445–473 (1988).
[20] Cho, J.H. and Lieuwen, T. "Laminar premixed flame response to equivalence ratio oscillations", *Combustion and Flame*, 140(1), pp. 116–129 (2005).
[21] Putnam, A., *Combustion Driven Oscillations in Industry*, Elsevier, New York (1971).
[22] Dowling, A.P. and Hubbard, S. "Instability in lean premixed combustors", *Journal of Power and Energy*, 214(4), pp. 317–332 (2000).
[23] You, D., Huang, Y. and Yang, V. "A generalized model of acoustic response of turbulent premixed flame and its application to gas-turbine combustion instability analysis", *Combustion Science and Technology*, 177(5), pp. 1109–1150 (2005).
[24] Huang, Y., Sung, H., Hsieh, S. and Yang, V. "Large-eddy simulation of combustion dynamics of lean-premixed swirl-stabilized combustor", *Journal of Propulsion and Power*, 19(5), pp. 782–794 (2003).
[25] Abu-Off, G.M. and Cant, R.S. "Reaction rate modeling for premixed turbulent methane-air flames", In *Proceedings of the Joint Meeting of Spanish, Portuguese*, Swedish and British Sections of the Combustion Institute, Madeira (1996).

Rouzbeh Riazi received his B.S. Degree in Thermo-Fluid Sciences from Amir Kabir University of Technology (Tehran Polytechnic). He obtained his M.S. Degree in Aerospace Engineering from Sharif University of Technology, Tehran, Iran, where he is currently studying for his Ph.D. Degree in the same subject. As researcher, he has also conducted an experimental study on Combustion Dynamics and NOx Emission of a Swirl Stabilized Combustor with Secondary Fuel Injection, in the Department of Mechanical and Aerospace Engineering at Tokyo Institute of Technology, Japan. His research interests include turbulent flame, combustion instability, combustion control, and droplet combustion analysis.

Mohammad Farshchi is a Professor in the Aerospace Engineering Department at Sharif University of Technology, Tehran, Iran. He received his Ph.D. in Mechanical Engineering from the University of California, Davis, USA. His research interests include combustion instability analysis, computational aero-acoustics, turbulent reacting flow analysis and droplet combustion analysis.